ADVANCED MATERIALS

reported elsewhere. This limits the peak brightness for this device to only 5500 cd m^{-2} (12 V). The ratio of excimer to monomer emission gradually becomes richer in monomer emission as the brightness is increased, analogous to the FIrpic-FPt1 WOLEDs. The CIE coordinates of approximately (0.34, 0.35) are not severely affected by the shift in the monomer–excimer ratio, remaining nearly ideal white up to ~2000 cd m^{-2}, with a CRI value at 75 or above for nearly all of the spectra considered. If we ignore the NPD emission, the CIE coordinates are slightly shifted to (0.33, 0.40). The CBP–FPt2 WOLEDs give $\eta_{ext} = 1.9 \pm 0.2$ % at a brightness of 100 cd m^{-2} ($J = 2$ mA cm^{-2}). The power efficiency at this brightness is 2.5 lm W^{-1}.

We have demonstrated that control of the molecular and electronic structures of an organic phosphor can lead to surprisingly efficient white light emission from an OLED containing only a single emissive dopant. We expect that these device structures will have several benefits over stacked or multiply doped single emissive layer devices.[6] The simple device structures make them well suited to low cost lighting applications. Indeed, a serious problem in multiple doped systems for white emission is differential aging. If one of the dopants degrades at a different rate from the others, the color of the device will change over time. This should not be the case for the single dopant monomer–excimer device. Degradation that results from charging or other reactions of the ground state molecules will equally affect the monomer and excimer emission. The photostability of these phosphorescent dopants is typically quite high, and device failure generally occurs through charged, rather than excitonic states.[19]

Experimental

The three phosphorescent dopants (FIrpic, FPt1, and FPt2) and NPD were prepared by literature procedures [20,21]. BCP and Alq_3 were purchased from Aldrich Chemical Company. PEDOT-PSS was purchased from Bayer Chemical. All of the molecular materials used to prepare WOLEDs were purified by thermal gradient sublimation before use.

Photoluminescent, photoluminescence excitation, and absorbance spectroscopy were performed on thin-films grown in vacuum ($< 1 \times 10^{-6}$ torr) by thermal evaporation on solvent-cleaned quartz substrates. The films were 1000 Å thick and were degassed with nitrogen during testing. Five films were grown: neat CBP, two films of CBP doped at < 1 wt.-% and ~7 wt.-% with FPt1, CBP doped with both FIrpic and FPt1 at 6 wt.-%, and CBP doped with 8 wt.-% of FPt2.

Electrophosphorescent double-doped monomer–excimer WOLEDs were grown with a 6 wt.-% FIrpic–6 wt.-% FPt1 doped CBP luminescent layer. The devices were fabricated on a glass substrate pre-coated with indium tin oxide (ITO, sheet resistance = 20 Ω/sq). The substrate cleaning and device fabrication were carried out by procedures described previously [6]. The device structure was ITO/PEDOT:PSS (400 Å)/NPD (300 Å)/CBP–FIrpic–FPt1 (300 Å)/BCP (500 Å)/LiF (5 Å)/Al (700 Å) (PEDOT:PSS=poly(ethylene-dioxythiophene): poly(styrene sulfonic acid), NPD=*N*,*N*′-diphenyl-*N*,*N*′-bis(α-napthyl)-4,4′-biphenyl, BCP=bathocuproine). A cross section of the device structure is shown in Figure 2. Devices were grown with areas as large as 2.7 cm^2 without loss in efficiency. The samples were exposed to air during tests. The device structure of the single dopant WOLEDs was ITO/NPD (400 Å)/CBP-8 wt.-% FPt2 (300 Å)/BCP (150 Å)/Alq_3 (200 Å)/LiF–Al (1000 Å).

Received: March 21, 2002
Final version: April 16, 2002

[1] L. S. Hung, M. G. Mason, *Appl. Phys. Lett.* **2001**, *78*, 3732.
[2] M. A. Baldo, D. F. O'Brien, Y. You, A. Shoustikov, S. Sibley, M. E. Thompson, S. R. Forrest, *Nature* **1998**, *395*, 151.
[3] C. Adachi, M. A. Baldo, M. E. Thompson, S. R. Forrest, *J. Appl. Phys.* **2001**, *90*, 5048.
[4] C. Adachi, M. A. Baldo, S. R. Forrest, S. Lamansky, M. E. Thompson, R. C. Kwong, *Appl. Phys. Lett.* **2001**, *78*, 1622.
[5] C. Adachi, R. C. Kwong, P. Djurovich, V. Adamovich, M. A. Baldo, M. E. Thompson, S. R. Forrest, *Appl. Phys. Lett.* **2001**, *79*, 2082.
[6] B. W. D'Andrade, M. E. Thompson, S. R. Forrest, *Adv. Mater.* **2001**, *13*, 147.
[7] J. Feng, F. Li, W. Gao, S. Liu, Y. Liu, Y. Wang, *Appl. Phys. Lett.* **2001**, *78*, 3947.
[8] X. Jiang, Z. Zhang, W. Zhao, W. Zhu, B. Zhang, S. Xu, *J. Phys. D: Appl. Phys.* **2000**, *33*, 473.
[9] J. Kido, H. Shionoya, K. Nagai, *Appl. Phys. Lett.* **1995**, *67*, 2281.
[10] M. Berggren, G. Gustafsson, O. Inganäs, M. R. Andersson, T. Hjertberg, O. Wennerström, *J. Appl. Phys.* **1994**, *76*, 7530.
[11] S. A. Jenekhe, J. A. Osaheni, *Science* **1994**, *265*, 765.
[12] N. J. Turro, *Modern Molecular Photochemistry*, University Science Books, Mill Valley, CA **1991**, Ch. 5.
[13] M. Pope, C. E. Swenberg, *Electronic Processes in Organic Crystals*, Oxford University Press, New York **1982**, Ch. 1.
[14] S. W. Lai, M. C. W. Chan, K. K. Cheung, C. M. Che, *Inorg. Chem.* **1999**, *38*, 4262.
[15] S. W. Lai, M. C. W. Chan, T. C. Cheung, S. M. Peng, C. M. Che, *Inorg. Chem.* **1999**, *38*, 4046.
[16] P. I. Kvam, M. V. Puzyk, K. P. Balashev, J. Songstad, *Acta Chem. Scand.* **1995**, *49*, 335.
[17] M. A. Baldo, C. Adachi, S. R. Forrest, *Phys. Rev. B* **2000**, *62*, 10 967.
[18] N. Tessler, N. T. Harrison, D. S. Thomas, R. H. Friend, *Appl. Phys. Lett.* **1998**, *73*, 732.
[19] Z. Popovic, H. Aziz, N. Hu, A. Ioannidis, P. d. Anjos, *J. Appl. Phys.* **2001**, *89*, 4673.
[20] J. Brooks, Y. Babayan, S. Lamansky, P. I. Djurovich, I. Tsyba, R. Bau, M. E. Thompson, *Inorg. Chem.* **2002**, in press.
[21] S. Lamansky, P. I. Djurovich, D. Murphy, F. Abdel-Razzaq, R. Kwong, I. Tsyba, M. Bortz, R. Bau, M. E. Thompson, *Inorg. Chem.* **2001**, *40*, 1704.

Metal Nanoparticles, Nanowires, and Contact Electrodes Self-Assembled on Patterned Monolayer Templates—A Bottom-up Chemical Approach**

By *Stephanie Hoeppener*, *Rivka Maoz*, *Sidney R. Cohen*, *Lifeng Chi*, *Harald Fuchs*, and *Jacob Sagiv**

Numerous studies of nanoscale materials such as metal and semiconductor nanoparticles,[1–8] nanowires,[8–11] nanotubes,[12,13] and various types of artificial supramolecular entities[14–19] carried out over the past decade have revealed exciting new electrical and optical properties, associated with size and spatial organization. These findings, and the vision of entire operational devices made of nanoscale compo-

[*] Prof. J. Sagiv, Dr. S. Hoeppener, Dr. R. Maoz
Department of Materials and Interfaces
The Weizmann Institute of Science
76100 Rehovot (Israel)
E-mail: jacob.sagiv@weizmann.ac.il
Dr. S. R. Cohen
Chemical Services Unit, The Weizmann Institute of Science
76100 Rehovot (Israel)
Dr. L. F. Chi, Prof. H. Fuchs
Physikalisches Institut, Westfälische Wilhelms-Universität
Wilhelm Klemm-Str. 10, D-48149 Münster (Germany)

[**] We thank Dr. Kazufumi Ogawa of Matsushita Electric Industrial Co. (Kyoto) for the supply of the NTS used in the fabrication of the thiolated layers, and Dr. Hagai Cohen of the Chemical Services Unit, WIS, for the XPS measurements. This research was supported by The Israel Science Foundation and Minerva Foundation (Germany).

  0935-9648/02/1508-1036 $ 17.50+.50/0

nents,[9,16,19–21] fuel the current growing interest in nanoscience and nanotechnology. To reach this major goal, it will, however, be necessary to develop advanced nanofabrication techniques, capable of precise and reliable handling of nanometric and sub-nanometric components of interest. This implies that future nanofabrication methods will have to largely rely on a "bottom-up" chemical approach.[16,19,21] A sufficiently general chemical approach, applicable to the planned assembly of a complete functioning device, does not yet exist. Its timeliness points to the urgency of systematic research aiming at the development of a coherent, self-consistent set of methods which, together, could constitute a basis for a genuine bottom-up nanofabrication paradigm. Here, we report a series of first experimental results demonstrating the feasibility of a comprehensive all-chemical strategy for the bottom-up fabrication and spatial fixation of some of the key components of a future nanoscale electric circuit—planned arrays of metal nanoparticles and metal nanowires electrically connected to addressable contact electrodes. All components, including the contact electrodes, are in-situ generated at predefined sites on a smooth silicon wafer surface, using processes of surface chemical derivatization and controlled self-assembly conducted on highly stable organic monolayer and bilayer template patterns. The fabrication of the template patterns themselves follows a similar all-chemical strategy based on surface self-assembly and site-selective surface chemical derivatization.

Our approach combines surface self-assembly with "*constructive nanolithography*", a recently discovered nanoelectrochemical patterning process that utilizes electrical pulses delivered by a conductive AFM tip for the non-destructive nanometer-scale inscription of chemical information (in the form of local chemical modification) on the top surfaces of certain highly ordered long-tail organosilane monolayers self-assembled on silicon.[22–24] Tip-induced oxidation of surface exposed vinyl ($-CH=CH_2$)[22] and methyl ($-CH_3$)[24] groups to hydroxyl-containing functions was demonstrated, as well as the reduction of Ag^+ ions, anchored to top thiol (–SH) functions, to elemental silver grains.[23] Both oxidized and reduced monolayer surface sites generated in this manner can participate in further self-assembly and chemical modification steps.[22–24] Of rather special significance, in this respect, is the tip-induced oxidation process converting top $-CH_3$ groups to –COOH.[24] Using, in the lithographic process, readily available organosilane monolayers with terminal $-CH_3$ groups offers virtually unlimited possibilities for site-controlled self-assembly and further chemical derivatization.[24] This follows from the fact that –COOH patterns generated in such monolayers by the lithographic process remain embedded within a chemically stable background of rather inert $-CH_3$ groups that are compatible with a wide variety of post-patterning chemical manipulations, thus allowing selective modification of the tip-affected sites only.[24] Particularly attractive for nanofabrication is the possible utilization of extremely robust organic film patterns (monolayers and thicker layered assemblies) produced in this manner as stable templates for precise control of the self-assembly pattern of selected inorganic materials such as metals and semiconductors.

The soundness of this approach draws on the analogy with natural processes of biomineralization, where fine tuning of the three dimensional (3D) structure of an inorganic species is achieved by controlled self-assembly on an optimally designed organic template scaffold.[25] Mimicking nature, successful control of crystal nucleation at well-defined interfaces has been demonstrated using ordered Langmuir,[26–29] Langmuir–Blodgett,[28,29] and self-assembled monolayers.[30,31] However, the complex issues involved in the development of template-controlled chemical processes that would allow the planned self-assembly of an entire functioning electric circuit of nanometric dimensions pose new and far more difficult scientific challenges. One major problem to be solved is concerned with the reproducible assembly of continuous, electrically conducting wires with nanometric lateral dimensions, connected to contact electrodes that can be addressed via a suitable input/output system. Another important issue has to do with the controllable fabrication of metal and semiconductor nanoparticles positioned at precisely predefined surface sites, i.e., lateral nanostructuring. Finally, all components of a practically useful nanometric circuit must be immobilized on the surface of a smooth solid substrate that can confer both high overall spatial stability and effective electrical insulation. To have real impact on future nanotechnologies, a useful bottom-up nanofabrication methodology should thus be capable of dealing satisfactorily with each of these key issues. In this communication we report a series of proof-of-concept experiments carried out with the purpose of demonstrating the practical feasibility of a comprehensive all-chemical nanofabrication strategy that can, in principle, meet this requirement.

A route for the in-situ chemical synthesis of predefined arrays of surface-immobilized gold nanoparticles on silicon, via hierarchical self-assembly from precursor CdS particles self-assembled on a patterned organic template, is demonstrated in Figure 1. The desired pattern of chemically active surface sites is first generated on the top surface of a dense, highly ordered OTS/Si monolayer (*n*-octadecyltrichlorosilane, self-assembled on a polished silicon wafer surface) by the tip-induced non-destructive nanolithographic process effecting the local electrochemical conversion of terminal methyls to carboxylic acid groups[24] (Fig. 1a). A second highly ordered monolayer with chemically reactive terminal ethylenic functions (NTS, nonadecenyltrichlorosilane)[22,24] is then allowed to selectively self-assemble on top of the patterned OTS monolayer, thus creating an elevated overlayer copy of the initial pattern of active monolayer sites inscribed by the tip[22,24] (Fig. 1b). The terminal ethylenic functions of NTS are subsequently photo-reacted with H_2S, to produce a thiolated top surface (Fig. 1c) consisting of a mixture of disulphide (–S–S–) and thiol (–SH) functions,[23,24,31] the latter acting as efficient binding sites for Cd^{2+} ions. CdS particles anchored to the bilayer pattern are then generated in a template-controlled self-assembly process, by exposing the Cd^{2+}-loaded surface to gaseous H_2S (Fig. 1d). Finally, conversion of CdS to metallic

  0935-9648/02/1508-1037 $ 17.50+.50/0

ADVANCED MATERIALS

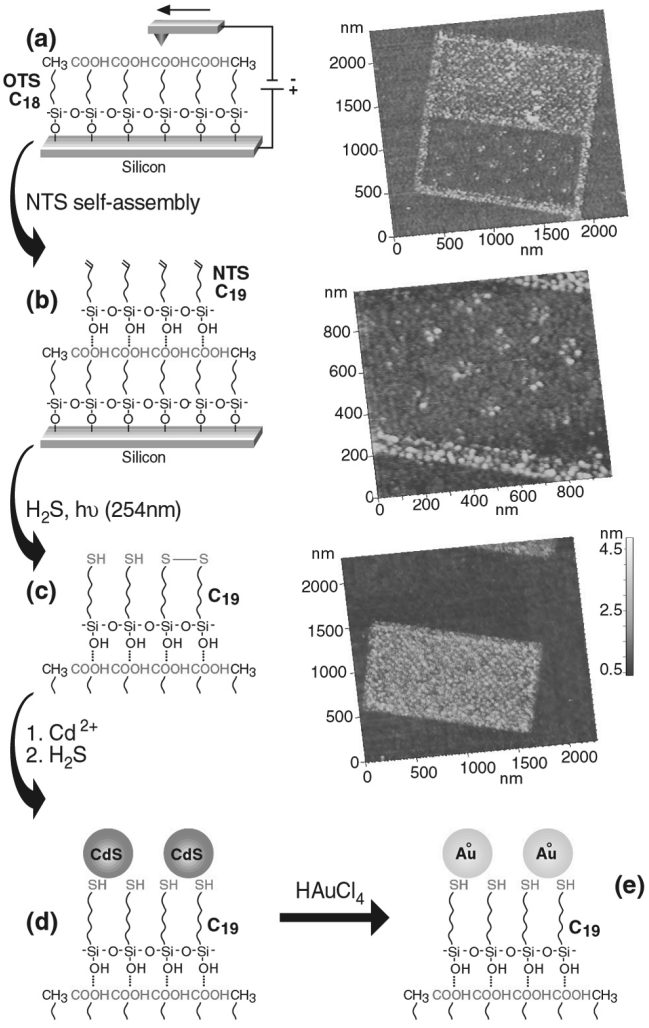

Fig. 1. Scheme of the hierarchical self-assembly of gold nanoparticles onto an organic bilayer template pattern on silicon, and examples of semicontact topographic AFM images of planned arrays of gold nanoparticles. Steps of the procedure are illustrated by sketches (a–e), see text and Experimental.

gold is achieved upon treatment with an aqueous solution of $HAuCl_4$ (Fig. 1e), via a redox chemical process involving the reduction of Au^{3+} to Au^0 and the oxidation of S^{2-} to S^0 ($3\ Cd^{2+}S^{2-} + 2H^+Au^{3+}Cl^-_4 \rightarrow 2\ Au^0 + 3S^0 + 3\ Cd^{2+}Cl^-_2 + 2H^+Cl^-$). The formation of elemental gold in this process was proved by the subsequent chemical deposition of metallic silver from a silver enhancer solution[23] on the gold treated surface. The silver deposition is catalyzed by metallic grains,[23] and does not occur in the presence of CdS only. Further confirming evidence was obtained from separate UV-vis absorption and X-ray photoelectron spectroscopy (XPS) measurements conducted on large area film samples of the same kind produced on optically transparent fused silica substrates. As expected, most of the $CdCl_2$ formed in the process dissolves in the acidic aqueous environment, only trace amounts of cadmium and chlorine being detected in the XPS measurements. Angle-dependent XPS data indicate the presence, on the treated surface, of sulphur covered by gold, the apparent sulphur concentration being ~2.5–3.0 times lower than the stoichiometric S^0/Au^0 ratio expected from the above redox process. This would suggest the formation of a rather unusual type of composite nanoparticles, with an outer gold shell surrounding an inner sulphur core.

As the AFM images in Figure 1 show, the formation of the gold particles is confined to the pattern of thiolated bilayer sites obtained as copies of the initial tip-inscribed –COOH monolayer sites, which demonstrates that the self-assembly of the inorganic material is indeed controlled by the organic template. Due to the strong adhesion of gold to the thiolated surface, the gold particles generated by the present process are faithful copies of the initially produced CdS particles (not shown). The characteristic average size and local lateral distribution of the latter are, in turn, controlled by the surface density of the Cd^{2+} binding sites and the lateral mobility of Cd^{2+} and CdS molecular species on the thiolated surface, which determine the kinetics of nucleation and growth of the CdS particles. It is, for example, interesting to observe that each of a number of isolated dots inscribed by the tip (Fig. 1, top and middle images) contains several discrete nanoparticles of comparable average size, but significantly smaller than the overall size of the tip-inscribed dot itself. While the lithographic dot size is mainly determined by the effective size of the AFM tip, it should thus be possible to chemically control the average size and number of nanoparticles generated within each lithographic dot by varying the surface concentration of the Cd^{2+} binding sites and the rate of lateral diffusion of Cd^{2+} and CdS species. This could, for example, be realized by using mixed monolayer templates with variable concentrations of thiol surface groups, and variable temperatures during the exposure to H_2S.

It should be noted that the procedure adopted here for the chemical generation of gold nanoparticles on a monolayer template represents one particular route among a number of different possible routes, each of which offering specific advantages for specific applications. These will be dealt with in forthcoming publications. The particular example now discussed serves to demonstrate the synthetic flexibility and reliability of the present chemical approach. Remarkably, the gold particles are generated via a sequence of five post-patterning chemical steps (Fig. 1), including the self-assembly of an NTS second layer on the patterned OTS monolayer, a gas-phase photochemical process, a gas-phase chemical process, and two wet chemical processes, all this without deterioration of the initial tip-inscribed information. The key step in this sequence is the site-selective assembly of a stable NTS overlayer, the top surface of which being then easily converted into a thiol-rich copy of the tip-inscribed pattern of carboxylic acid groups. This strategy provides a convenient path not only for the transfer of the lithographic information to a template suitable for the assembly and anchoring of CdS and gold particles, it also suggests interesting possibilities for planned layer-by-layer build-up of 3D nanoarchitectures, starting from an initial monolayer pattern.

Millimeter-size silver electrodes that can be used for electrical contact with a nano-size electric circuit were assembled by the chemical route depicted in Figures 2a–f.

  0935-9648/02/1508-1038 $ 17.50+.50/0

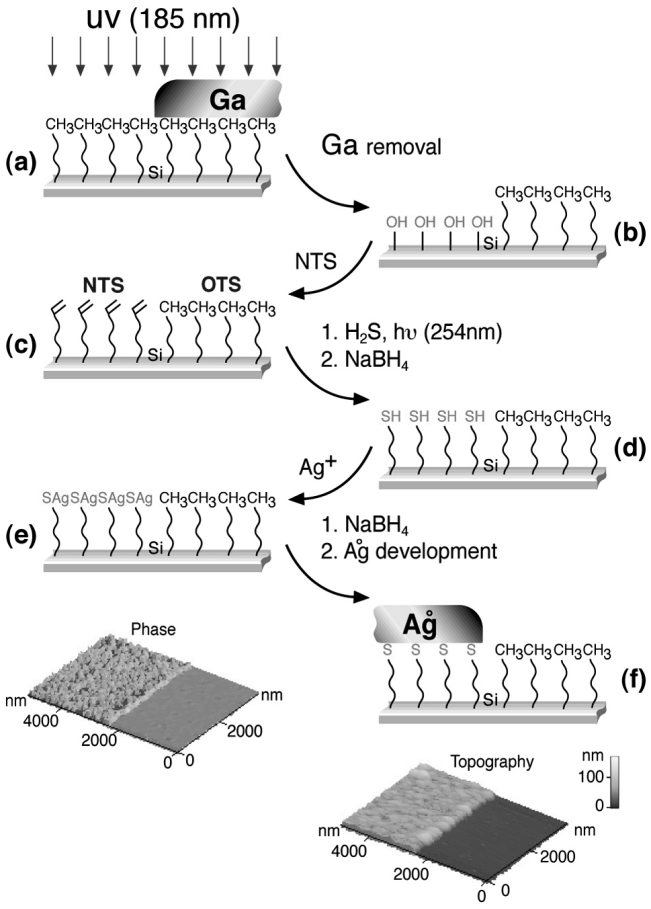

Fig. 2. Schematic view of the guided self-assembly of a millimeter-size silver contact electrode on a top-thiolated silane monolayer template bordering an OTS-covered region on silicon (steps a–f), and simultaneously recorded semicontact mode topographic and phase AFM images of the edge region of an electrically conducting electrode, fabricated by this procedure (see Experimental).

This process was designed to create a molecularly sharp boundary between a surface region coated with a top-thiolated silane monolayer, intended to serve as both template for the silver self-assembly and efficient silver adhesion coupler to the underlying silicon surface (Fig. 2e,f), and an OTS-coated region on which template patterns for the subsequent self-assembly of the desired electric nanocircuit components could be inscribed with a conductive AFM tip. It would be difficult to meet all these requirements using conventional lithography. In the present chemical process, molecularly sharp boundaries were easily generated by monolayer photodesorption,[32] a drop of supercooled liquid gallium being used as an opaque semisolid contact mask that does not wet and does not adhere to the OTS surface while maintaining molecular contact with it, and which can be mechanically manipulated to form a sharp air-liquid-solid three-phase contact line (Fig. 2a). Silver metal self-assembles selectively on the thiolated portion of the surface produced through the steps shown in Figure 2b–d, a sharp boundary being maintained with the OTS-covered area due to the high hydrophobicity of the OTS surface, which prevents its wetting by the aqueous reagents applied during the silver self-assembly steps (Figs. 2d–f, see Experimental). The resulting polycrystalline silver electrode is electrically conducting and displays the expected sharp boundary at the edge of the OTS-covered surface region (see AFM images in Fig. 2, and lateral conductivity imaging experiments described with reference to Fig. 4).

Polycrystalline silver wires, ~6 μm long, 40–70 nm wide (as deduced from the AFM data, which may overestimate lateral size because of the convolution with the tip) and ~25 nm thick, emanating from a millimeter-size silver electrode (assembled as described above) and ending in separate micron-size contact electrodes, were fabricated by the direct silver metal self-assembly on –COOH template patterns "written" with the AFM tip (Fig. 3). A step-by-step cyclic procedure involving in-situ chemical reduction of Ag^+ ions bound to the

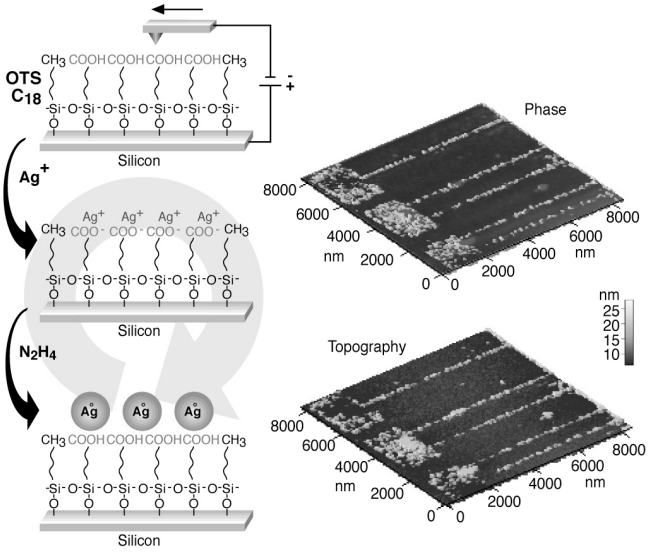

Fig. 3. Left side: scheme of the controlled self-assembly of silver micro- and nanofeatures on a monolayer template pattern produced by the direct lithographic action of the AFM tip. Right side: simultaneously recorded semicontact mode topographic and phase AFM images of micrometer-size silver electrodes and nanowires fabricated by the process indicated in the scheme (see Experimental).

top carboxylate functions of the template was used to generate variable densities of surface-anchored silver nanoparticles (Fig. 3, left side). These were further developed with a silver enhancer solution (not shown),[23,24] in order to fill up intergrain gaps and thus produce a continuous metal structure. By the end of the metal growth protocol (Fig. 3 and Experimental), unfilled gaps are still visible both within the area of the electrodes and along the wire tracks (Fig. 3, AFM images). These gaps can be filled up by repeating parts of the metal growth process employed, however, this would also add to the lateral size of those portions of the wires that have already reached continuity. Recent preliminary results point to the possible formation of metal nanowires with more uniform and smaller cross sections, by using other types of functionalized template patterns and metal self-assembly processes.

Lateral conductivity imaging experiments with self-assembled nanostructures of interconnected silver wires and electrodes (emanating, like those of Fig. 3, from a millimeter-size self-assembled contact electrode) were carried out as

  0935-9648/02/1508-1039 $ 17.50+.50/0

ADVANCED MATERIALS

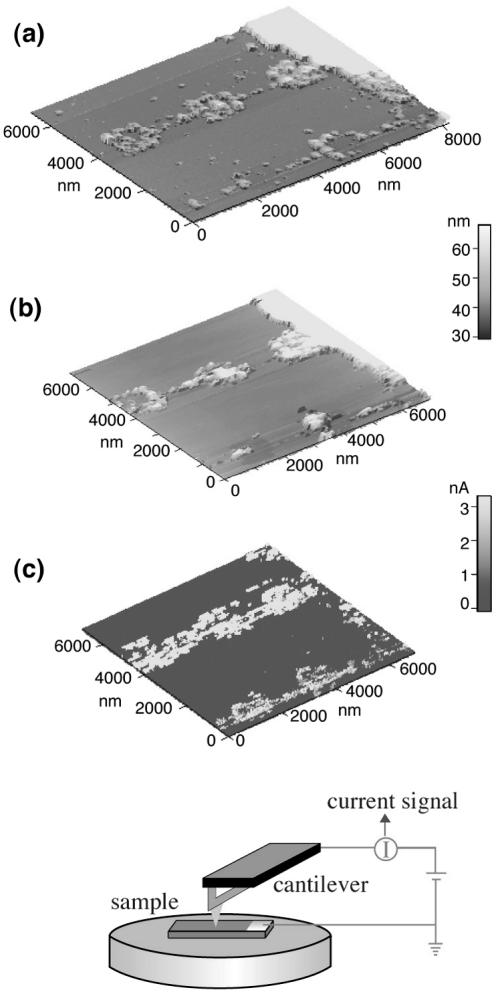

Fig. 4. Lateral conductivity imaging experiments. a) Semicontact mode topographic AFM image of a self-assembled silver pattern consisting of interconnected nanowires and micrometer-size electrodes touching the edge of a millimeter-size contact electrode (visible in the upper-right extremity of the image). The silver features were fabricated by controlled self-assembly on a monolayer template (on silicon), as described in Figures 2 and 3. b,c) Simultaneously recorded contact mode topographic and respectively lateral current images of the silver patterns shown in (a) obtained with a conductive W_2C-coated probe under a lateral bias of 5.0 V applied between cantilever and the millimeter-size contact electrode, as depicted in the scheme of the experimental set-up.

shown in Figure 4, using same type of tungsten carbide-coated conductive tips as in the nanoelectrochemical patterning of the base OTS monolayers. Contact mode images (Figs 3b,c), taken with the lateral bias on, appear somewhat degraded compared with the initial semicontact image (Fig. 3a), taken without lateral bias, and some of the features visible in the current image (Fig. 3c) are not observed in the corresponding topographic image (Fig. 3b). This is caused by the electrooxidation of the W_2C tip coating under the relatively high current flow in these experiments, which mainly affects the resolution of the current imaging, and the shear-induced lateral displacement of tiny metal grains during the contact mode scans. Thus, some of the silver grains that contribute to lateral current are not evident on the topographic scale set by the much larger silver features present in the scanned area. Despite these experimental difficulties, a comparison of the three images in Figure 4 unequivocally demonstrates the confinement of lateral current to the silver pattern, thus providing convincing qualitative evidence for the electrical conductivity of these self-assembled metal structures.

The template-assisted self-assembly approach illustrated with the present examples focuses on four basic elements, regarded as necessary or particularly advantageous for the rational advancement of a viable bottom-up nanofabrication paradigm: i) the use of stable, highly ordered organosilane monolayers as building blocks in the assembly of the organic templates provides, besides functional diversity, the required structural robustness and electrical insulation, as well as an inherently well adapted means for the achievement of subnanometric precision in the definition of template features; ii) the use of smooth silicon as substrate material is a logical ideal choice for many practical applications; iii) in conjunction with properly selected schemes of surface chemical derivatization, AFM can become a useful nano-analytical tool, not only for structural characterization, but also for the chemical identification of the various nano-size objects assembled on the surface; iv) relying on an essentially all-chemical self-assembly strategy, with only minimal intervention by the AFM in the initial pattern imprinting step, the present approach to nanofabrication offers unusual synthetic flexibility, adaptable to the handling of diverse materials of interest. Although not yet optimized, the specific experimental protocols applied during this study serve to emphasize both the conceptual and practical significance of the proposed chemical approach, and particularly its wide synthetic potential. Bringing to fruition this inherent capability is a challenge for future research.

Experimental

The self-assembly of the base OTS and top NTS layers was carried out as described before [22], by complete immersion of the bare or monolayer-coated silicon specimens in the respective silane solutions (5 mM) in pure bicyclohexyl (BCH), followed by sonication in analytical-grade toluene. The silicon substrates were cut, as before [24], from double-side-polished p-type silicon wafers (Semiconductor Processing Co., 0.5 mm thick, orientation <100>, resistivity 8–11 Ω cm).

Millimeter-size silver electrodes were assembled as follows (Fig. 2a–f): a–b) a drop of liquid gallium was placed on the OTS/Si surface at ~70 °C and then flattened out (while cooling down to the ambient temperature) with the tip of a glass pipette so as to cover the desired portion of the monolayer surface. UV irradiation ($\lambda = 185$ nm, ~40 min) was carried out with the Hg-vapor lamps of a UV/O_3 cleaner (model NL-UV 253, NLE, Nagoya, Japan) operated in a pure argon atmosphere, in order to avoid formation of ozone that could affect the non-irradiated portion of the OTS monolayer. Gentle mechanical removal of the supercooled semisolid gallium layer from the surface, immersion of the sample for ~5 min in aqueous HCl (5 %), rinse in pure water for ~5 min, and final blow off of the water film wetting the UV-exposed area with clean N_2 completed the monolayer photodesorption step (see text); b–d) self-assembly of an NTS monolayer and its subsequent photochemical conversion to a layer with top thiol and disulphide groups, as in Figure 1. To reduce the –S–S– groups to –SH, the sample was immersed in an aqueous $NaBH_4$ solution (50 mM) for ~10 min, rinsed in pure water and finally blown dry with clean N_2 [31]; d–e) the loading of the thiolated monolayer with Ag^+ ions (to yield a silver thiolate surface) was done by immersing the sample for ~15 min in a 1 mM aqueous solution of silver acetate, followed by a short rinse with ethanol and final blow off of the residual liquid with clean N_2 [23,31]; e–f) reduction of the surface bound Ag^+ ions with aqueous $NaBH_4$, performed as in step (c–d), and subsequent development (with a silver enhancer solution [23,24]) of the resulting metal grains to a continuous silver

  0935-9648/02/1508-1040 $ 17.50+.50/0

metal film. To maintain a sharp boundary with the OTS-covered region, a sufficiently large drop of the aqueous silver enhancer solution was placed on the hydrophobic portion of the surface (in the OTS-covered region) and then pushed with the tip of a pipette until being spontaneously and quantitatively sucked into the thiolated region, at the contact line between the two monolayer regions. This surface energy-driven phenomenon occurs because of the very high hydrophobicity (low surface energy) of the OTS (water contact angle ≈115°, advancing as well as receding), compared with that of the thiolated layer (advancing angle ≈60°, receding angle ≈30°). The development process was stopped, after a few minutes of exposure to the silver enhancer solution, by sucking most of the liquid with a piece of clean filter paper. Several rinses with drops of pure water were then performed in the same manner, starting from the OTS-covered region, the residual water on the silver film being let to evaporate under a dust cover. Weakly bound surface contaminants were finally removed with a piece of Scotch tape before taking the AFM images, without any visible damage being caused to the silver electrode or to its sharp boundary at the OTS-covered region.

Controlled self-assembly of silver micro- and nanofeatures on a monolayer template pattern produced by the direct lithographic action of the AFM tip (Figs. 3,4): the nanolithographic inscription of the –COOH pattern on OTS/Si is followed by loading of the patterned surface with Ag^+ ions (in the same manner as the Ag^+ loading of the thiolated surface (Figs. 2d,e) to produce the silver carboxylate salt). The reduction of the Ag^+ ions to elemental silver (yielding metallic silver nanoparticles and the regeneration of free –COOH surface groups) was done with hydrazine (N_2H_4) vapor, by placing the sample for ~10 min above a small beaker containing hydrazinium hydroxide ($N_2H_5^+OH^-$), in a closed glass vessel immersed in a water bath at ~40 °C [31]. The sample was finally rinsed in a water overflow and blown dry with clean nitrogen. The two-step silver generation cycle was repeated five times, after which the silver nanoparticles accumulated on the surface were mildly developed with a silver enhancer solution [23,24] (not shown). The nanowires connect the micron-size electrodes to the edge of a millimeter-size silver electrode (visible at the right side extremity of the images) fabricated by the process described in Figure 2.

Patterns were "written" with conductive W_2C-coated silicon tips (Silicon-MDT) in a controlled humidity atmosphere (65–70 % relative humidity, obtained by mixing dry and wet nitrogen), using contact mode raster lithography (minimal contact forces, 9–10 V positive sample bias relative to the tip, 3.5–3.7 ms/pixel). The AFM images were taken in the ambient atmosphere, in the semicontact mode, with regular silicon probes (Silicon-MDT). A SOLVER P47 instrument (NT-MDT, Moscow, Russia) was used for both patterning (with the lithographic software provided by the manufacturer) and imaging. Lateral conductivity images were obtained in the contact mode, as described in Figure 4.

Received: March 6, 2002
Final version: April 28, 2002

[1] *Nanoparticles and Nanostructured Films* (Ed: J. H. Fendler), Wiley-VCH, Weinheim **1998**.
[2] C. B. Murray, C. R. Kagan, M. G. Bawendi, *Annu. Rev. Mater. Sci*. **2000**, *30*, 545.
[3] A. C. Templeton, W. P. Wuelfing, R. W. Murray, *Acc. Chem. Res.* **2000**, *33*, 27.
[4] K. C. Grabar, K. J Allison, B. E. Baker, R. M. Bright, K. R. Brown, R. G. Freeman, A. P. Fox, K. D. Keating, M. D. Musick, M. J. Natan, *Langmuir* **1996**, *12*, 2353.
[5] M. M. Alvarez, J. T. Khoury, T. G. Schaaff, M. N. Shafigullin, I. Vezmar, R. L. Wetten, *J. Phys. Chem. B* **1997**, *101*, 3706.
[6] G. Markovich, C. P. Collier, S. E. Henrichs, F. Remacle, R. D. Levine, J. R. Heath, *Acc. Chem. Res.* **1999**, *32*, 415.
[7] L. F. Chi, M. Hartig, T. Drechsler, T. Schwaak, C. Seidel, H. Fuchs, G. Schmid, *Appl. Phys. A* **1998**, *66*, S187.
[8] G. Schmid, L. F. Chi, *Adv. Mater*. **1998**, *10*, 515.
[9] Y. Huang, X. Duan, Q. Wei, C. M. Lieber, *Science* **2001**, *291*, 630.
[10] C. Durkan, M. E. Welland, *Phys. Rev. B* **2000**, *61*, 14 215.
[11] C. Durkan, M. A. Schneider, M. E. Welland, *J. Appl. Phys.* **1999**, *86*, 1280.
[12] T. W. Ebbesen, H. J. Lezec, H. Hiura, J. W. Bennett, H. F. Ghaemi, T. Thio, *Nature* **1996**, *382*, 54.
[13] *Science and Application of Nanotubes* (Eds: D. Tománek, R. Enbody), Kluwer Academic/Plenum, New York **2000**.
[14] W. Fudickar, J. Zimmermann, L. Ruhlmann, J. Schneider, B. Röder, U. Siggel, J.-H. Fuhrhop, *J. Am. Chem. Soc.* **1999**, *121*, 9539.
[15] S. A. Levi, P. Guatteri, F. C. J. M. van Veggel, G. J. Vaneso, E. Dalcanale, D. N. Reinhoudt, *Angew. Chem. Int. Ed.* **2001**, *40*, 1892.
[16] A. N. Shipway, E. Katz, I. Willner, *ChemPhysChem* **2000**, *1*, 18.
[17] T. P. Cassagneau, B. Sweryda-Krawiec, J. H. Fendler, *MRS Bull.* **2000**, *25*, 40.
[18] Y. Lu, Y. Yang, A. Sellinger, M. Lu, J. Huang, H. Fan, R. Haddad, G. Lopez, A. R. Burns, D. Y. Sasaki, J. Shelnutt, C. J. Brinker, *Nature* **2001**, *410*, 913.
[19] V. Balzani, A. Credi, M. Venturi, in *Stimulating Concepts in Chemistry* (Eds: F. Vögtle, J. F. Stoddart, M. Shibasaki), Wiley-VCH, Weinheim **2000**, pp. 255–266.
[20] H. Ahmed, *J. Vac. Sci. Technol. B* **1997**, *15(6)*, 2101.
[21] J. R. Heath, *Acc. Chem. Res.* **1999**, *32*, 388.
[22] R. Maoz, S. R. Cohen, J. Sagiv, *Adv. Mater.* **1999**, *11*, 55.
[23] R. Maoz, E. Frydman, S. R. Cohen, J. Sagiv, *Adv. Mater.* **2000**, *12*, 424.
[24] R. Maoz, E. Frydman, S. R. Cohen, J. Sagiv, *Adv. Mater.* **2000**, *12*, 725.
[25] H. A. Lowenstam, S. Weiner, *On Biomineralization*, Oxford University Press **1989**.
[26] E. M. Landau, M. Levanon, L. Leiserowitz, M. Lahav, J. Sagiv, *Nature* **1985**, *318*, 353.
[27] S. Mann, B. R. Heywood, S. Rajam, J. D. Birchall, *Nature* **1988**, *334*, 692.
[28] E. M. Landau, S. Grayer Wolf, M. Levanon, L. Leiserowitz, M. Lahav, J. Sagiv, *J. Am. Chem. Soc.* **1989**, *111*, 1436.
[29] J. H. Fendler, F. C. Meldrum, *Adv. Mater.* **1995**, *7*, 607.
[30] J. Aizenberg, A. J. Black, G. M. Whitesides, *Nature* **1999**, *398*, 495.
[31] E. Frydman, *Ph.D. Thesis*, Weizmann Institute, September **1999**.
[32] W. J. Dressick, J. M. Calvert, *Jpn. J. Appl. Phys.* **1993**, *32*, 5829.

Ultralow-*k* Dielectrics Made by Supercritical Foaming of Thin Polymer Films**

By *Bernd Krause*, *Geert-Henk Koops*, *Nico F. A. van der Vegt*,* *Matthias Wessling*, *Michael Wübbenhorst*, and *Jan van Turnhout**

There is an urgent need for low- and ultralow-*k* dielectric materials. The present insulation materials such as silicon dioxide exhibit *k* values of 3.9–4.2) (*k* denotes the relative permittivity, which is often also symbolized by ε). Future generation materials require dielectric constants below 2.2.[1–3]

Non-polar polymers allow us to conquer the low-*k* region,[2,3] nonetheless only a few polymers meet the mechanical strength and temperature requirements. In the quest for lowering the permittivity of polymers down to ultralow-*k* values, several research groups are exploring the incorporation of nanosized air cells. Current initiatives are based on two principles: i) thermal decomposition of a block copolymer made of a thermally stable block and a thermally unstable one,[4–7] ii) thermolysis of high glass-transition temperature (T_g) polymers blended with thermally labile fillers (polymers or organic components).[8,9]

[*] Dr. N. F. A. van der Vegt, Dr. B. Krause,[+] Dr. G. H. Koops, Prof. M. Wessling
University of Twente, Membrane Technology Group
P.O. Box 217, NL-7500 AE Enschede (The Netherlands)
E-mail: n.f.a.vanderVegt@ct.utwente.nl
Prof. J. van Turnhout, Dr. M. Wübbenhorst
Delft University of Technology, Polymer Materials and Engineering
Julianalaan 136, NL-2628 BL Delft (The Netherlands)
E-mail: j.vanturnhout@tnw.tudelft.nl
[+] Present address: Gambro Dialysatoren GmbH & Co. KG, Membrane & Device Research, Holger-Crafoord-Str. 26, D-72379 Hechingen, Germany.

[**] M. Chalid and P. J. Droppert are gratefully acknowledged for assistance with the dielectric measurements.

  0935-9648/02/1508-1041 $ 17.50+.50/0